RSC Applied Interfaces

ROYAL SOCIETY OF CHEMISTRY

PAPER

View Article Online
View Journal

Cite this: DOI: 10.1039/d5lf00290g

Fine-tuning the surface coverage of niobium oxide on platinum catalysts and its impact on the oxygen reduction reaction

Annabelle M. K. Hadley, Jennie I. Eastcott, Abhinav Parakh, Michael T. Y. Paul, Matthew W. Bilton, Austin W. H. Lee and Byron D. Gates *

Received 25th September 2025,
Accepted 7th January 2026

DOI: 10.1039/d5lf00290g

rsc.li/RSCApplInter

Platinum electrocatalysts coated with an ultrathin film of niobium oxide, which were prepared with a fine-tuned surface coverage, were evaluated for their influence on the oxygen reduction reaction. A series of ultrathin (<10 nm thick), patterned coatings of niobium oxide were prepared on planar platinum substrates using a combination of atomic layer deposition, photolithography, and wet-chemical etching techniques. Atomic layer deposition enabled a high degree of control over the thickness of the niobium oxide coating. Niobium oxide is a corrosion-resistant material that can improve the stability of electrocatalysts. A balance is sought, though, between the stabilizing benefits of applying a metal oxide coating to electrocatalysts and the possible blockage of catalytically active sites. The study presented herein pursues a method to precisely tune the surface coverage of niobium oxide coatings using techniques to pattern these coatings on a platinum electrocatalyst. The prepared catalysts were evaluated using a range of electrochemical and microscopy techniques. It was found that catalysts with higher coverages of niobium oxide had a higher initial resistance towards the oxygen reduction reaction but significantly outperformed the long-term performance of the uncoated, pristine platinum catalyst.

Introduction

Many industries are interested in developing electrocatalysts capable of long-term use, particularly for catalysts composed of precious materials such as platinum. Platinum nanoparticles on carbon supports are leading in their performance as cathode catalysts in hydrogen-based polymer electrolyte membrane fuel cells (PEMFCs), but still suffer from some key degradation mechanisms that can wreak havoc on device performance in the long term.[1] Specifically, Pt cathode catalysts are prone to dissolution in strongly acidic fuel cell conditions when successively oxidized and reduced.[2–4] Corrosion of the carbon support is also a known source of performance loss over time in fuel cells.[5,6] There have been attempts to minimize these mechanisms to increase catalyst stability using metal oxide supports or coatings.[7–12] Reducible metal oxides, including TiO_2, SiO_2, and Nb_2O_5, are more resistant to corrosion in acidic conditions and have been shown to improve the stability of fuel cell catalysts when incorporated as supporting materials.[13–17] These metal oxides improve nanoparticle catalyst stability by forming a thin (angstrom- to nano-scale) layer that can fully or partially cover the catalyst surfaces and utilize strong metal support interactions.[18,19] The low electrical conductivity of metal oxides compared to carbon particles is, however, one of the barriers towards commercializing these strategies to improve the stabilization of Pt electrocatalysts.

The benefits of metal oxide supports can be extended to nanocatalysts supported on carbon substrates or nanostructured Pt thin films (*e.g.*, nanostructured catalysts developed by 3 M and others)[20,21] through the creation of thin metal oxide coatings. These catalyst designs would bypass the conductivity shortfalls of the metal oxides, allowing electron conduction to occur through the C and/or Pt. Coatings come with their own benefits and challenges. A coating prepared from metal oxides would create a protective barrier to Pt dissolution.[22–24] For example, it can enable the transport of oxygen and protons associated with the electrocatalytic reaction but can hinder the transport of solvated metal ions. Heterogeneous catalysts contain active sites across their surfaces, and covering these surfaces can decrease their activity if the coating lacks sufficient porosity or is too thick to allow transport or an adequate rate of transport of reactants to access the surfaces of the catalyst. Some prior art has investigated the effects of altering the porosity and thickness of an encapsulating layer on the activity of the underlying catalyst, primarily using silica-based

Department of Chemistry, Simon Fraser University, 8888 University Drive, Burnaby, BC V5A 1S6, Canada. E-mail: bgates@sfu.ca

coatings.[9,11,12,25–28] These studies demonstrated that sufficiently porous, thin coatings can produce catalyst designs that are more durable and can also match the activity of pristine, uncoated catalysts.

The activity of a coated catalyst can also be maintained by modifying the surface coverage of the overlayer to achieve a balance between increasing the catalyst durability, a quality imparted by the coating, and catalyst accessibility by designing pathways to the catalyst surfaces.[29] Fabrication of well-defined and patterned coatings is commonly achieved using atomic layer deposition (ALD) due to this technique's high control over film thickness. Ultrathin metal oxide coatings applied *via* ALD have been shown to improve the activity,[30–33] stability,[30–32] and selectivity[34] of electrocatalysts. Strides are being made as well to improve the viability of atomic layer deposition at the commercial scale.[35] Partial overlayers composed of metal oxides, including Al_2O_3, SiO_2, ZrO_2, and TiO_2, can improve the stability of supported nanoparticle catalysts in harsh reaction environments, increase yields for targeted chemical products, and protect catalyst surfaces from contaminants such as sulfur and carbon.[36–39] The coatings can realize these results by improving adherence of the catalyst to the support, minimizing catalyst movement and dissolution, blocking particular facets of the catalysts to alter reaction specificity, and moderating accessibility of reagents or contaminants (*e.g.*, determined by the size of pores in the coating). Partial coatings can also modify the catalyst's surface properties, such as its wettability, depending on the coverage of the overlayer.[40] In the prior work, nanoscale thin films of Nb_2O_5 were shown to modestly improve the durability of planar Pt catalysts.[7] It is of interest to better understand the role of the niobium oxide coating and the influence of changes in its relative surface coverage on the activity and durability of the Pt catalyst. This work builds upon the prior art by exploring the effects of a well-defined decrease in the surface coverage of ultrathin Nb_2O_5 on a Pt catalyst. Methods were utilized to create niobium oxide coatings with well-defined patterned features. A set of catalysts coated with ultrathin films of Nb_2O_5 was prepared such that the overlayer achieved a fine-tuned surface coverage ranging from 0% (pristine Pt) to ~65% (partially covered Pt). The partial coverage of the niobium oxide coating was achieved using a combination of ALD and microscale patterning techniques. The creation of microscale features in the niobium oxide coating enabled a relatively simple means of tracking the durability of this coating and assessing the influence of well-defined amounts of Pt exposed to the electrolyte. Transformations to the patterned Nb_2O_5 layer and the Pt electrocatalysts were evaluated as a function of a series of electrochemical tests. In contrast, nanoscale features would be more challenging to fabricate, and, alternatively, creating a mesoporous ultrathin niobium oxide film would present challenges in tracking transformations to the niobium oxide relative to the Pt electrocatalyst as a function of the electrochemical tests. These studies demonstrated, for example, that the durability of the Pt catalysts improved with an increase in the coverage of the ultrathin coating of Nb_2O_5. The results presented herein highlight the importance of continuing to develop custom-designed coatings on electrocatalysts as a strategy to enhance their durability.

Results and discussion

Characterization of electrocatalysts coated with ultrathin films of patterned Nb_2O_5

Planar platinum electrocatalysts coated with patterned, ultrathin films of Nb_2O_5 were evaluated herein relative to the activity and durability of pristine Pt electrodes. This study assessed the influences of niobium oxide layers with either of two specific patterns, each with a well-defined surface coverage of Nb_2O_5, on the electrocatalytic performance of the Pt. The custom-prepared niobium oxide coatings contained distinct patterns that enabled the fine-tuning of the surface area of the Pt in direct contact with the electrolyte. Photolithography and wet-chemical etching techniques were used for their ability to create reproducible, well-ordered structures. These techniques can also be scaled up to produce these structures over larger areas and to prepare many samples reproducibly.[41] Combining these photolithography techniques with ALD of niobium oxide, Pt catalysts were prepared with clearly defined patterned coatings of Nb_2O_5 (Fig. S1). X-ray photoelectron spectroscopy measurements of the coated Pt sample confirmed the presence of Nb_2O_5 based on the binding energies of Nb 3d (Fig. S2, Table S1). Two types of distinct patterns were pursued herein, as depicted in Fig. 1. The scanning electron microscopy (SEM) images in Fig. 1 depict the patterned niobium oxide on the Pt electrodes due to the contrast resulting from differences in secondary electrons (as well as the backscattered electrons) produced from regions of exposed Pt catalyst and regions of Nb_2O_5-coated Pt. In these SEM images obtained by measuring the secondary electrons, the areas of the Pt substrate coated with an ultrathin layer of Nb_2O_5 have a darker appearance compared to areas of bare, exposed Pt. The Nb_2O_5 film patterned with a hexagonal array of circular holes exposed the underlying Pt through these circular openings, each with a diameter of ~4 μm (Fig. 1a and c). The complementary pattern consisted of a hexagonal array of circular islands of Nb_2O_5, each with a diameter of ~5 μm, covering the Pt electrode (Fig. 1b and d). These patterns remained visible and largely intact even after extensive electrochemical cycling [*i.e.*, 5000 cycles of the applied potential from 0 to 1.3 V (*vs.* RHE) while immersing the electrodes in a sulfuric acid electrolyte], with no substantive morphological differences observed in the appearance of the circular Nb_2O_5 islands or holes. The diameter of the arrays of circular holes did not change following this durability test, exhibiting a consistent diameter of 3.8 ± 0.1 μm before and after the durability test (Fig. S3). The circular islands did show a slight decrease in the nominal diameter of these features following the

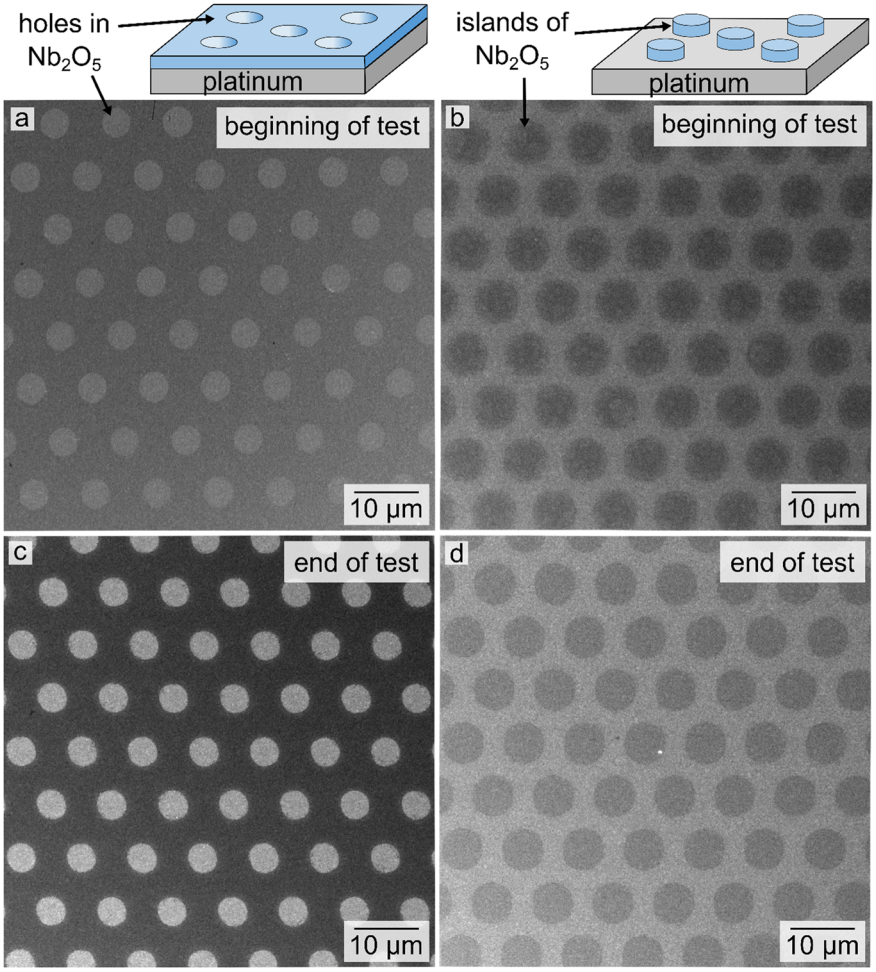

Fig. 1 Scanning electron microscopy (SEM) images of platinum (Pt) capped with patterned niobium oxide (Nb_2O_5) films containing either (a and c) hexagonal arrays of circular holes in the Nb_2O_5 or (b and d) hexagonal arrays of circular islands of Nb_2O_5. The SEM images were obtained (a and b) before and (c and d) after performing a durability test [*i.e.*, 5000 cycles of the applied potential from 0 to 1.3 V (*vs.* RHE) while immersing the electrodes in a sulfuric acid electrolyte].

extensive electrochemical cycling (*e.g.*, shifting from 5.5 ± 0.2 μm to 5.3 ± 0.2 μm as shown in Fig. S3, with the sample variance reported to one standard deviation from the mean value). Although these values are not statistically significant, it is possible that a slight change in diameter could result from a loss of material from the outermost portions of these circular islands. The edges of these features may not have been as firmly adhered to the Pt substrate following the ALD and lift-off process, which utilized the lithographically defined features. During the prolonged electrochemical treatment, any poorly adhered features could be removed from the Pt substrate. Another explanation, although less likely due to the uniform appearance of the features in SEM, is that some photoresist residue may have been retained at the edges of the features that subsequently dissolved or delaminated over the course of the durability testing. Interestingly, the majority of the patterned Nb_2O_5 features remain intact after extensive electrochemical cycling, suggesting an otherwise firmly adhered coating.

The patterned features in the niobium oxide coated Pt samples were further analyzed using atomic force microscopy (AFM) and Kelvin probe force microscopy (KPFM). The results of these analyses demonstrated an agreement with the dimensions of the patterned features as measured from the SEM images (Fig. 2). The AFM images were, however, insufficient to distinguish the patterned features from the topography of these polycrystalline Pt electrodes when observed by cross-sectional analyses. The grain sizes of the Pt are such that the roughness of these films (~20 nm) is greater than the thickness of the ultrathin niobium oxide coating (~5 nm). A subtle difference in the height of the patterned islands of Nb_2O_5 relative to the planar Pt electrocatalyst can be seen in the compiled AFM image (Fig. 2c). In contrast, the KPFM imaging readily distinguishes the coated and pristine regions in these electrodes with its ability to differentiate the work function between the two types of surfaces (*i.e.*, Pt and Nb_2O_5), generating a high-contrast image. These analyses confirm that the patterned Nb_2O_5 layers are sufficiently thick and conformal to alter the

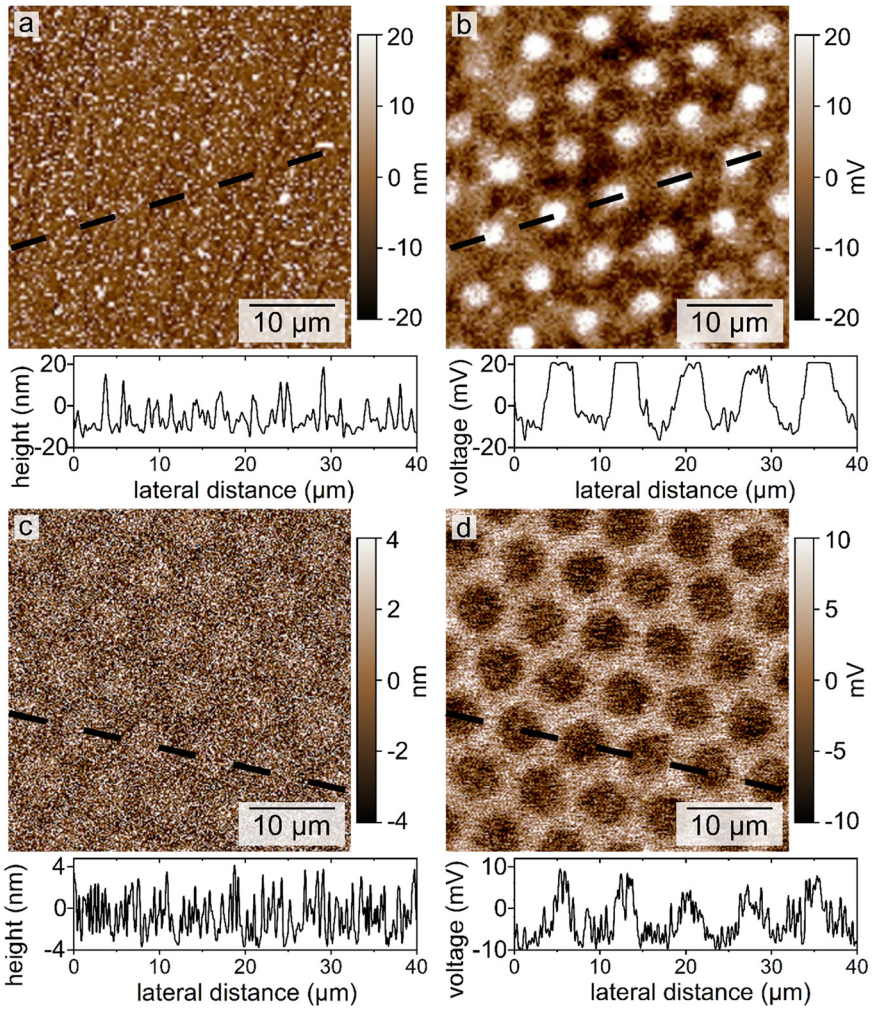

Fig. 2 (a and c) Atomic force microscopy (AFM) images of the topography and (b and d) Kelvin probe force microscopy (KPFM) maps of patterned, ultrathin Nb_2O_5 coatings on polycrystalline, planar Pt as observed after a series of electrochemical tests. These samples contained (a and b) arrays of circular holes in the Nb_2O_5 coating or (c and d) arrays of circular Nb_2O_5 islands on the Pt. Height and voltage profiles below each image correspond to the regions indicated by the dashed lines.

electrical conductivity of the substrate. Exposed regions of Pt exhibited a KPFM signal that was ~15 to 30 mV higher than that obtained for the areas coated by an ultrathin layer of Nb_2O_5. This difference in KPFM signal was attributed to the higher work function of polycrystalline Pt (5.64 eV) relative to that of bulk Nb_2O_5 (5.2 eV).[42,43]

Although the thickness of the Nb_2O_5 layers could not be accurately determined by AFM techniques, due to the ultrathin nature of these films and the roughness of the Pt electrodes, additional techniques were utilized to confirm the composition and structure of these patterned ultrathin coatings. A more accurate determination of the thickness of the niobium oxide coatings was sought by preparing cross-sections of the Pt electrodes coated with an ultrathin, patterned layer of Nb_2O_5. Sections from the sample were lifted out and thinned using focused ion beam (FIB) assisted processes for analysis by transmission electron microscopy (TEM). Specifically, cross-sections isolated from the samples were analyzed using scanning transmission electron microscopy (STEM) and energy dispersive X-ray spectroscopy (EDS) techniques (Fig. 3). An EDS map displaying the overlapping elemental compositions (Fig. 3d) further supports the formation of an ultrathin coating of Nb_2O_5 (in cyan) on the Pt electrode (in red). The Ir layer (blue) was used to protect the sample's surfaces during the FIB-assisted preparation of the thin cross-sections. The Nb_2O_5 film deposited by ALD appears not to have an atomically precise thickness on the polycrystalline Pt electrodes. These electrodes were relatively rough as they were prepared by physical vapour deposition (PVD) techniques. This non-uniformity in the thickness of the niobium oxide coating may result from the roughness of the Pt substrate and any trapped water present on these surfaces during the ALD processes used to create the ultrathin coatings (Fig. S4a). Another study also observed non-uniformities in ultrathin (<5 nm thick) metal oxide films deposited by ALD on metal substrates prepared by PVD. In this case, it was posited that the non-uniformity

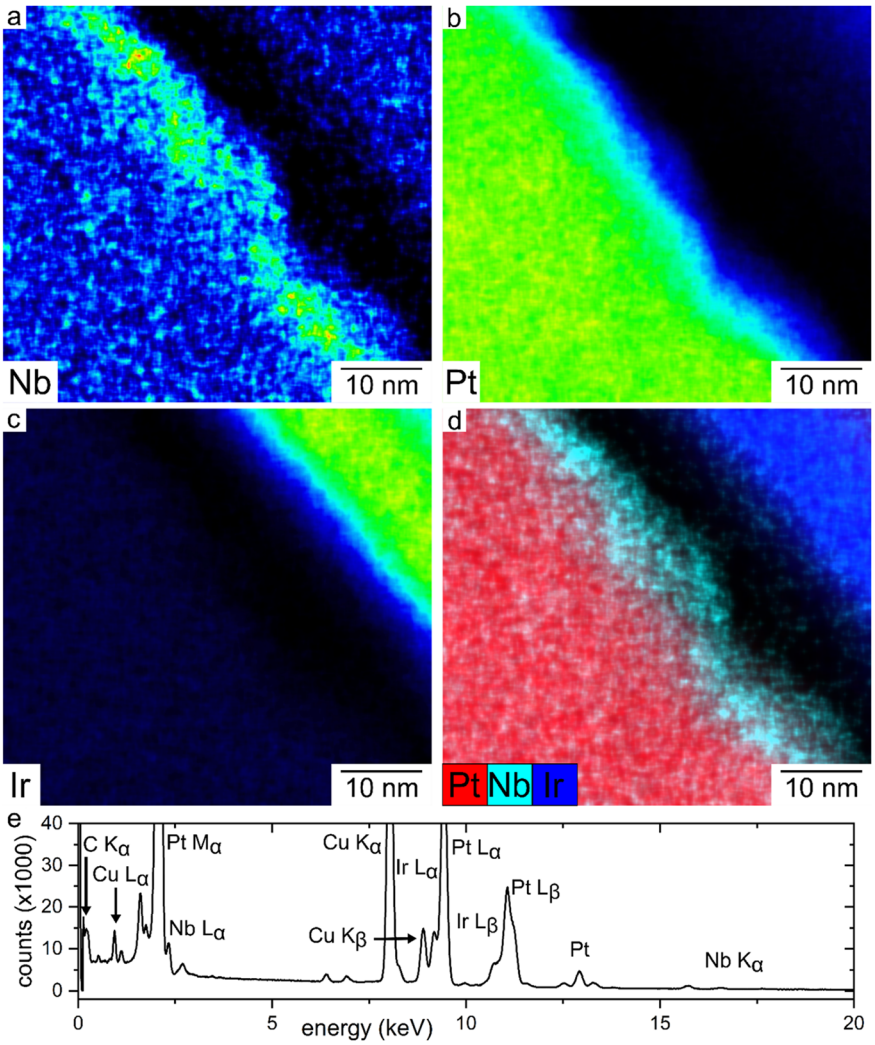

Fig. 3 (a–c) Individual and (d) overlapping elemental maps for the (a) Nb Kα, (b) Pt Lα, and (c) Ir signals as obtained by energy dispersive X-ray spectroscopy (EDS) measurements of a cross-section obtained from a Nb_2O_5 coated polycrystalline Pt substrate. (e) A representative spectrum obtained using EDS techniques with labelled transitions.

was due to preferential deposition in valleys between the grains of the metal substrate.[22] In contrast, coatings created by ALD on atomically smooth surfaces, such as on faceted or finely polished single-crystalline materials, can exhibit highly uniform and conformal coatings.[44] The highly textured surfaces of polycrystalline materials create features that could trap water or other species, even under high vacuum processes.[45] Ultrahigh vacuum and elevated temperatures are often required to remove such surface residue.[46,47] Trapped water or residue on the surfaces could create preferential sites for initiating niobium oxide formation. The observed non-uniformities in the thickness of the coatings may also be influenced by the conditions required to create sufficiently thin cross-sections for the STEM analyses (*e.g.*, FIB milling procedures). These are relatively minor features in the overall sample, though, as the fabrication and thin film deposition processes used herein were sufficient to obtain highly regular arrays of patterned features and sufficiently conformal coatings for both masking the electronic properties of the underlying Pt substrate (Fig. 2b and d) and for the patterned coatings to adhere to the Pt throughout their subsequent electrochemical treatment (Fig. 1c and d). The thickness of the Nb_2O_5 layer, as estimated from the EDS analyses, was 5 to 9 nm, thicker than the targeted thickness of ~3 nm. The actual thickness of the ALD-prepared film is likely influenced by moisture or residue trapped at the surfaces and the variable topography of the Pt substrate. There could also be overlapping signals from the Nb and Pt due to the thickness of the cross-sections being proportional to the size of some Pt grains (*e.g.*, conformal niobium oxide coatings covering the surfaces of a Pt grain could lead to overlapping signals during EDS analysis). In summary, this estimation of the film thickness is likely to be overestimated. However, it confirms the presence of an ultrathin niobium oxide coating on the polycrystalline Pt substrates and the conformal nature of these ultrathin films.

Performance and stability of Pt electrodes coated with patterned Nb_2O_5 features

The performance and stability of the patterned coatings on the Pt electrocatalysts were evaluated using a series of electrochemical techniques. The patterned niobium oxide coatings increased the electrocatalysts' hydrophobicity, as measured by their advancing and receding water contact angles, relative to the pristine Pt electrocatalyst (Table S2). However, the Nb_2O_5 modified samples remained sufficiently hydrophilic to be efficiently wet by the electrolyte throughout these electrochemical tests. The results of the electrochemical tests for the custom electrocatalysts coated with patterned arrays of niobium oxide were compared to the performance of pristine, uncoated Pt electrocatalysts. Before and after these electrochemical tests, each sample was characterized using cyclic voltammetry (CV) to assess the electrochemically active surface area (A_{ecsa}). The surfaces of the coated and uncoated samples were also probed with potassium ferricyanide to further evaluate the accessibility of the Pt electrode. In addition, linear sweep voltammetry (LSV) measurements were performed under oxygen-saturated conditions to study the electrodes' activity towards the oxygen reduction reaction (ORR). Analyses were conducted using electrochemical impedance spectroscopy (EIS) to assess the charge transfer resistances and capacitances of each sample. The series of electrochemical tests for each sample included subjecting these custom-prepared electrodes to 5000 cycles of an accelerated stress test to rigorously evaluate their durability. These studies aimed to collectively understand the impact of applying patterned arrays of ultrathin microscale features on the electrochemical performance of the Pt electrocatalyst, and to specifically investigate variations in these effects on their ORR activity and Pt durability.

Results of the cyclic voltammetry analyses (Fig. 4a) exhibit features associated with hydrogen underpotential deposition (H_{UPD}) on Pt (~0.05 to 0.4 V_{RHE}) and Pt oxide reduction (~0.6 to 1.0 V_{RHE}) for each of the niobium oxide coated and the pristine, uncoated Pt electrocatalysts. As expected, the magnitude of the response decreases for the electrocatalysts with patterned niobium oxide coatings compared to the same electrochemical features observed for the pristine, uncoated

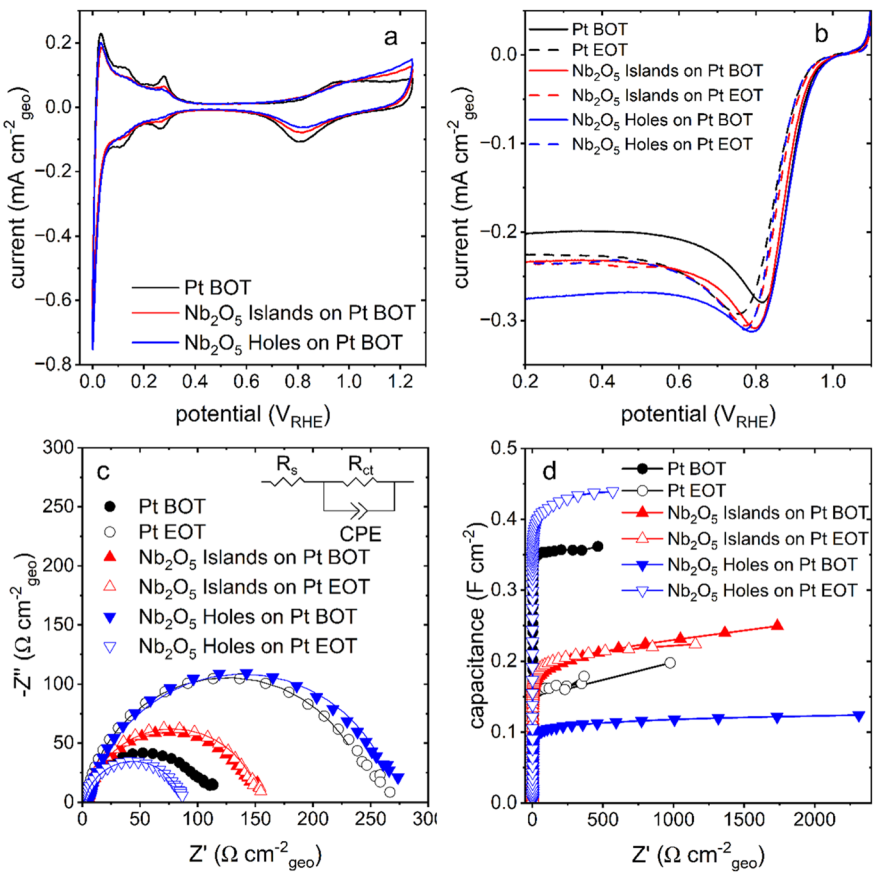

Fig. 4 (a) A series of cyclic voltammetry plots corresponding to Pt catalysts (pristine or with patterned Nb_2O_5 coatings) before a durability test (BOT). (b) Linear sweep voltammetry plots obtained with an O_2 (g) saturated electrolyte before (BOT, solid line) and after (EOT, dashed line) this durability test. (c) Nyquist plots recorded at 0.9 V_{RHE} in O_2 saturated electrolyte at BOT (solid symbols) and EOT (hollow symbols) with fits (solid lines) corresponding to the inset circuit. (d) Capacitance plots derived from electrochemical impedance spectroscopy at 0.4 V_{RHE} in N_2 (g) saturated electrolyte at BOT (solid symbols) and EOT (hollow symbols). Colours correspond to bare Pt (black), and arrays of circular islands (red) or circular holes (blue) in a Nb_2O_5 film on Pt.

Pt electrocatalyst. However, these differences in the CV plots for this series of electrocatalysts became negligible after electrochemical cycling (Fig. S5). The A_{ecsa}, calculated by integrating the hydrogen adsorption region, was initially smaller for the patterned electrodes, decreasing with an increase in the surface coverage of the ultrathin coating of Nb_2O_5 on the Pt surface (Table 1). These results suggest that the Nb_2O_5 layer had a measurable impact on the accessibility of the electrolyte to the Pt catalyst. However, reagents are being transported through the Nb_2O_5 film to the catalyst surface, which is consistent with the observations made in prior art.[9,12] The observed decrease in A_{ecsa} due to applying the patterned coating was not equivalent to the loss predicted solely based on the geometric surface coverage of these niobium oxide films. For instance, relative to the pristine Pt, samples containing arrays of circular Nb_2O_5 islands and arrays of circular holes in a Nb_2O_5 film contained ~65% and ~30%, respectively, of the Pt electrocatalyst in direct contact with the electrolyte. In contrast, these samples retained ~84% and ~77%, respectively, of the A_{ecsa} relative to the pristine, uncoated Pt (each normalized by its respective geometric surface area). The trend in the A_{ecsa} is mirrored in a plot comparing the capacitance of each sample at the beginning of the electrochemical tests or beginning of test (BOT) (Fig. 4d). These results further support the decrease in A_{ecsa} associated with a decrease in exposed regions of Pt as determined by the lithographically defined templates used to pattern the niobium oxide layers. The activity of the catalysts towards the ORR was evaluated from LSV plots and EIS measurements. The results for the BOT in the LSV measurements exhibited similar overpotentials across all types of electrodes, differing by less than 20 mV at −0.03 mA cm^{-2}_{geo} (Fig. 4b). The overpotentials were compared in the mixed diffusion and kinetic controlled region of the LSV (−0.03 mA cm^{-2}_{geo}), the region of interest for ORR catalysts.[48] These results may indicate that the ultrathin films of niobium oxide are participating in the ORR as well, given that niobium oxide and niobium oxide doped with Pt have exhibited some ORR activity.[49] On the other hand, the Nyquist plots reveal striking differences between the three electrode morphologies (Fig. 4c). The coverage of Nb_2O_5 has a substantial impact on the charge transfer resistance towards the ORR. This impact can be easily visualized in the changes to the diameter of the semi-circle of the Nyquist plots, which grows larger with increased coverage of Nb_2O_5.

The surfaces of the samples were probed with potassium ferricyanide *via* cyclic voltammetry at different scan rates (Fig. S6). The peak current of the pristine Pt catalyst increased linearly with the square root of the scan rate, while the peak currents of the patterned catalysts only linearly increased at scan rates up to 200 mV s^{-1} (Fig. S7). At lower scan rates, the CV plots are similar in shape and peak separation, regardless of whether a patterned coating is present. Davies *et al.* observed similar results when studying electrodes that were patterned with inactive regions.[50] When the inactive zones are small and closely spaced relative to the radial diffusion of the active species, as is the case for the Nb_2O_5 patterned Pt electrodes, then the patterned electrode behaves like a pristine electrode. Although it has been shown that ultrathin niobium oxide layers are permeable to protons and oxygen in previous work,[7] this could explain the similarity in the CVs even if the ferricyanide ion is less able to penetrate the niobium oxide layer. The CVs of the Pt sample patterned with an array of holes in the Nb_2O_5 layer (*i.e.*, a higher surface coverage of Nb_2O_5) have smaller currents than the corresponding CVs of the other two samples. This is likely a result of the much higher coverage of the Nb_2O_5 in this sample [~70% coverage compared to ~35% and 0% coverage of the samples in (b) and (a), respectively]. The ferricyanide probe is a larger molecule than the protons used to measure the A_{ecsa}, and so the lower current may be due to a lower permeability of the ferricyanide through the niobium oxide layer than protons. Furthermore, as the scan rate increases, CV peaks of the patterned electrodes broaden, and the peak current no longer increases linearly with the square root of the scan rate (Fig. S7). At higher scan rates, species have less time to diffuse radially to uncoated sections of the electrode. If the niobium oxide did not pose a barrier to the ferricyanide probe, no decrease in peak current would be observed at high scan rates since the electrode would remain accessible regardless of the coating. However, the non-linearity in the peak currents observed in Fig. S7 at the highest scan rate for the coated samples suggests some blocking behaviour.[51] The broadening of the peak is evidence of a combination of the response of the electrochemical reaction occurring at the

Table 1 Electrochemically active surface area (A_{ecsa}) and charge transfer resistance (R_{CT}) before (BOT: beginning of test) and after (EOT: end of test) 5000 sequential cyclic voltammetry scans of a bare, uncoated Pt electrode (Pt), and samples coated with a patterned layer containing either circular islands of Nb_2O_5 or circular holes in a Nb_2O_5 coating exposing the underlying Pt substrate

Sample	Bare Pt surface area (%)	BOT[a] A_{ecsa} (cm^2 cm^{-2}_{geo})	EOT[b] A_{ecsa} (cm^2 cm^{-2}_{geo})	Change in A_{ecsa} with cycling (%)	BOT R_{CT} (Ω cm^{-2}_{geo})	EOT R_{CT} (Ω cm^{-2}_{geo})
Bare, planar Pt	100	1.46 ± 0.05	1.1 ± 0.1	−24 ± 5	106 ± 2	247 ± 6
Nb_2O_5 islands on Pt	~65	1.23 ± 0.02	0.988 ± 0.007	−19.5 ± 0.5	147 ± 3	152 ± 3
Holes in Nb_2O_5 on Pt	~30	1.12 ± 0.01	1.16 ± 0.01	+3.72 ± 0.06	266 ± 5	85 ± 2

[a] BOT = beginning of test (after conditioning and initial electrochemical cycling). [b] EOT = end of test (after extensive electrochemical cycling).

surface of the bare Pt regions and at the regions of the Pt coated by niobium oxide.[50]

The impact of the patterned niobium oxide coatings on the catalyst stability was evaluated by subjecting each of the electrodes to a 5000-cycle stress test, as was also pursued in a previous study of Nb_2O_5 coated Pt catalysts.[7] After completing the conditioning and other aspects of the BOT, the electrocatalysts were cycled from 0 to 1.3 V (*vs.* RHE) at 200 mV s^{-1} while immersed in a sulfuric acid electrolyte. The catalysts were subsequently characterized by additional electrochemical measurements, and the results were compared with the properties of the catalysts before this stress test. Overall, an increased coverage of Nb_2O_5 improved the retention of the A_{ecsa} in the electrocatalysts (Table 1). Rapid and repeated oxidation and reduction of Pt are known to result in the formation of Pt oxides and Pt dissolution, which can lead to Pt re-structuring when dissolved Pt ions re-deposit on the electrode surface.[52,53] This is the likely mechanism behind the measured change in the A_{ecsa} of the pristine Pt electrocatalyst. These results suggest that the Nb_2O_5 layer effectively stabilizes the Pt surfaces, potentially by preserving the size of the Pt grains and, consequently, their A_{ecsa}. Potential changes to the grain size of the exposed polycrystalline Pt relative to the Pt underneath the niobium oxide coating are not distinguishable by the microscopy methods used herein (Fig. S4b–e). This trend could also result from losing the Nb_2O_5 coating throughout the testing. Analysis of the coated samples pre- and post-AST by XPS did not suggest a loss of the Nb_2O_5 coating, as indicated by the intensity of the Nb 3d signal. Furthermore, SEM imaging showed that the dimensions of the patterned features in the Nb_2O_5 coatings closely match those in the as-prepared samples (Fig. 1). The substantial decrease observed in the charge transfer resistance of the samples containing arrays of patterned holes in the Nb_2O_5 films after the prolonged electrochemical cycling was not the result of a loss of the Nb_2O_5 coating (Table 1). The decrease in the charge transfer resistance may also be attributed to Pt doping of the niobium oxide coating, although evidence of this doping was not observed by XPS (Fig. S8, Table S1). This doping could occur as Pt atoms were removed from the catalyst's surfaces during the aggressive oxidizing and reducing conditions of the stress test, subsequently migrating into or out of the niobium oxide layer and re-depositing on the metal oxide surface. Migration of dissolved Pt ions and subsequent re-deposition is a well-established degradation mechanism in hydrogen fuel cells.[54] The presence of Pt throughout the niobium oxide coating would explain the decrease in the charge transfer resistance of the coated sample. Future analyses of cycled Pt catalysts with niobium oxide coatings using Auger electron spectroscopy, a technique with a higher surface sensitivity than XPS, may help detect changes in the composition and oxidation state of surface species. Since some studies have shown little electronic interaction between Nb_2O_5 and platinum,[55,56] this would explain a lack of changes in the Nb 3d XPS spectrum and any changes in the Pt 4f spectrum may have been overshadowed by the bulk Pt. Additional computational studies, coupled with further experiments on Pt electrodes with niobium oxide thin film coatings, could help to elucidate the mechanism behind these results.

The electrodes containing an array of Nb_2O_5 islands on the Pt electrode also exhibited an improved A_{ecsa} retention relative to the pristine, uncoated Pt catalyst. Crucially, the samples with niobium oxide islands exhibited no change in their charge transfer resistance throughout the electrochemical tests. In contrast, the pristine Pt electrocatalyst showed a substantive increase in charge transfer resistance. This increase reflects changes in the surface composition of the sample. The increased charge transfer resistance is partially explained by normalization of the data to the geometric surface area. The A_{ecsa} of the pristine Pt sample decreased by ~24% after the durability testing, and normalizing the EIS data to the A_{ecsa} accounts for this change (Fig. S9). Normalizing the data to the A_{ecsa} does not result in any changes to the trend in the samples overall, though the increase in the charge transfer resistance of the pristine Pt sample is less exaggerated. The cause of the remaining increase was studied *via* XPS analysis. The XPS spectrum of the pristine Pt post-AST did not show clear evidence of the formation of resistive platinum oxides (Fig. S10 and S11, Table S1). However, sulfur was detected in the survey scan. Sulfur species are known to negatively impact the ORR activity of Pt catalysts, and their presence would lead to an increased charge transfer resistance. The presence of the sulfur was unexpected, as the conditioning cycles conducted after the AST should have been sufficient to remove any contaminants from the catalyst surface.[57] This provides a further example of the benefit of the niobium oxide coating as an anti-fouling coating since the sulfur was not detected in the coated sample post-ADT (Fig. S11).

Conclusions

This paper successfully demonstrated the preparation and electrochemical performance of Pt electrocatalysts containing ultrathin coatings of Nb_2O_5 with distinct arrays of patterned features. These ultrathin coatings of niobium oxide were prepared by atomic layer deposition, and the patterns were prepared from these coatings using a combination of photolithography and wet-chemical etching techniques. The resulting hexagonal arrays of features in the niobium oxide coating enabled both a discernment of the influence of defects in this coating on the electrochemical activity and durability of the Pt electrocatalysts, as well as tracking the regions coated with niobium oxide to monitor changes in their properties as a function of electrochemical cycling. The presence and thickness of these Nb_2O_5 coatings were investigated using FIB lift-out assisted methods and STEM and EDS analyses. The patterned features within the ultrathin coating of niobium oxide were confirmed using KPFM and SEM techniques. The electrochemical activity and durability of pristine, polycrystalline platinum electrocatalysts towards

the ORR were compared to two types of samples with patterned coatings of niobium oxide (*i.e.*, one containing a hexagonal array of circular holes and the other containing a hexagonal array of circular niobium oxide islands). The features in these patterned niobium oxide coatings were found to be robust and remained essentially unchanged after extensive electrochemical cycling. As expected, an increase in the relative coverage of the Nb_2O_5 layer led to a decrease in the initial A_{ecsa} and an increase in the charge transfer resistance. In contrast, the key finding for durability was that higher coverages of the Nb_2O_5 film substantively improved the retention of A_{ecsa} in the samples following the stability test. These results point to the ability of these ultrathin metal oxide films to improve the Pt electrocatalyst's stability.

Experimental methods

Fabrication of platinum substrate by physical vapour deposition (PVD)

Polished silicon (Si) wafers were used as a substrate to support the Pt electrocatalysts prepared by physical vapour deposition (PVD), as previously described.[7] Briefly, four-inch diameter, p-type, test-grade, single-side-polished (100) Si wafers with a resistivity between 1 and 10 Ω cm were purchased from 4D LABS at Simon Fraser University (SFU). The Si wafers were cleaned in a Class 100 clean room with a sequence of acetone, isopropyl alcohol, and oxygen plasma (Technics, PEII-A) at 280 mTorr and 300 W of plasma to remove organic residue from the surface for improved adhesion of the deposited films. Metal deposition was performed using a PVD system (Kurt J. Lesker PVD75) with the chamber pressure $<2.00 \times 10^{-6}$ Torr. A ~5 nm thick Cr layer was deposited using thermal evaporation to ensure sufficient adhesion between the Si wafer and the Pt layer. Without breaking vacuum, the Pt layer was deposited using an electron beam-assisted evaporation technique with a target thickness of ~200 nm. The thickness of thin films during the deposition was monitored using a quartz microbalance (Sigma SQM-242) installed within the PVD system.

Fabrication of ultrathin Nb_2O_5 films by atomic layer deposition (ALD)

Ultrathin films of Nb_2O_5 were prepared *via* a thermally assisted ALD process using a Cambridge NanoTech Fiji F200 in 4D LABS at SFU as previously described.[7] Briefly, the reaction chamber was placed under vacuum and purged with high purity Ar gas (99.999%, Praxair). The Pt-coated Si substrates (each measuring ~2 cm × 2 cm) were loaded into the ALD chamber for a sequential reaction with tert(butylimino)tris(diethylamido)niobium (TBTDEN) and H_2O as precursors. The chamber and precursor temperatures were set to 250 °C and 65 °C, respectively, and the pressure was held at 0.0156 Torr in the main chamber. The Ar carrier gas and Ar plasma flow rates were set to 60 sccm and 200 sccm, respectively. The TBTDEN was introduced into the chamber for 1 s, followed by introducing argon gas for 0.5 s. After three of these cycles, the H_2O was introduced to the chamber for 0.06 s followed by a 0.5 s Ar gas purge. This process was repeated a total of 270 times to achieve the desired target thickness. The growth rate for the Nb_2O_5 film was determined *vide infra* to be 0.1 Å per cycle under these reaction conditions. The Nb_2O_5 film thickness was targeted to be 3 nm using 270 cycles.

Fabrication of patterned Nb_2O_5 films *via* lithography and buffered oxide etching

The ALD thin films of Nb_2O_5 covered Pt were further processed by photolithographic techniques to create arrays of circular features (*e.g.*, holes or islands) in the thin Nb_2O_5 layer to selectively expose portions of the underlying Pt surface. To create these periodic structures, a photomask with the desired patterns was used to project the pattern onto the photoresist (PR) layer upon the Nb_2O_5-coated Pt substrate. After developing the patterns in the PR coated substrates, these samples were subjected to a wet chemical etch using a buffered hydrofluoric acid to selectively remove the un-masked Nb_2O_5 thin film to create the desired patterns. A schematic of this process is displayed in Fig. S1. The preparation of the Nb_2O_5 patterns consisted of the following steps: (1) wash the Nb_2O_5-coated Pt substrate thoroughly with isopropanol and subsequently wash with deionized water; (2) bake the substrate on a hotplate at 110 °C for 1 min to dehydrate the surface; (3) spin cast AZ® MiR™ 703 (Microchemicals, Germany) over the substrate at 4500 rpm to create ~1 μm thick film of PR; (4) bake the PR coated substrate at 90 °C for 1 min to remove excess solvent from the film of PR; (5) expose the PR coated substrate using a UV-mask aligner (OAI MB800) through a chrome/borate glass photomask (fabricated by 4D LABS at SFU, Burnaby, BC, Canada) for a duration of 1.3 s; (6) bake the exposed PR at 110 °C for an additional 1 min; (7) fully immerse the exposed PR into ~100 mL of AZ® 300 MIF developer (Microchemicals, Germany) for ~1 min; (8) rinse the substrate thoroughly with deionized water and dry under a flow of filtered N_2 gas; (9) immerse the dried substrate into a solution of 10 : 1 Buffered Oxide Etchant (hydrofluoric acid based BOE, J.T. Baker, NJ, USA) for 30 s. *Caution: hydrofluoric acid is highly corrosive. The necessary safety protocols must be followed when working with this acid*; (10) rinse the etched substrate thoroughly with deionized water; (11) rinse the substrate with 10 mL of isopropanol for ~10 s to remove the PR mask; and (12) rinse the substrate thoroughly with deionized water and dry under a flow of filtered nitrogen gas.

Focused ion beam (FIB) milling and scanning electron microscopy (SEM)

The thickness of the Nb_2O_5 films prepared by ALD was evaluated using a FIB lift-out procedure with an FEI Helios Dual-Beam SEM located in 4D LABS at Simon Fraser University. The method outlined in Eastcott *et al.* was

followed herein.[7] Briefly, prior to milling and to protect the surface with a material that would not interfere with the analysis of the sample (*e.g.*, Pt), an ~16 nm thick layer of C and an ~20 nm thick layer of Ir were coated onto the sample with a Leica EM ACE600 high-vacuum sputter coater. Finally, the gas injection system within the Dual-Beam SEM was used to deposit an additional protective layer composed of Pt through assistance with the FIB. A Ga ion beam was used to initially mill an ~10 μm × ~2 μm × ~3 μm cross-section that was further thinned to ~30 nm while attached to an Omniprobe copper lift-out grid.

Kelvin probe force microscopy (KPFM) and atomic force microscopy (AFM) analyses

To examine surface topography and changes in work function for the ultrathin films scanning probe microscopy techniques, including Kelvin Probe Force Microscopy (KPFM), were performed using an MFP-3D-SA Atomic Force Microscope (Asylum Research) operating in an AC mode using silicon cantilevers from Asylum Research (Electrilever Model no. AC240TM, f_o of 70 kHz, k of 2 N m^{-1}) with a Cr and Pt coating with thicknesses of 5 nm and 20 nm, respectively, and a tip radius of 28 nm. Images were acquired from scan areas of 40 μm by 40 μm with a scan speed of 0.33 Hz and a resolution of 256 by 256. The images were analyzed using Igor Pro 6.22.

Water contact angle measurements

The advancing and receding water contact angles were measured for each type of sample. Ultrapure water (18.2 MΩ cm) was used for these measurements, applying 1 μL aliquots to the same position on a sample to measure a series of advancing angles. The receding contact angle measurements were obtained after removing 1 μL aliquots from this same position on the sample. The reported contact angles were obtained by calculating the average and standard deviation from approximately five advancing and four receding contact angle measurements, while including the values measured on both sides of each droplet. In addition, each set of measurements was averaged over two or three regions of the sample that had been in contact with the electrolyte solution during the electrochemical measurements. These measurements were performed after electrochemical cycling to investigate the differences in contact angles after any electrochemical activation of the surfaces of each electrocatalyst.

X-ray photoelectron spectroscopy

The X-ray photoelectron spectroscopy (XPS) based spectra were collected using a Kratos Axis Ultra system equipped with a monochromatic Al Kα source and a delay line detector (DLD). Measurement under high vacuum required the samples to be secured to a copper sample bar. The survey scans were acquired over binding energies (BE) from 1200 eV to 0 eV and a flood gun was used as a charge neutralizer. During data analysis, the binding energies of the high-resolution spectra were calibrated to the adventitious C 1s peak at 284.8 eV and a Shirley fit background subtraction was applied using CasaXPS software (version 2.3.16).

Half-cell electrochemical analysis

Electrochemical measurements were performed at 25 °C with a Metrohm Potentiostat (Model PGSTAT 302 N) using a three-electrode system in 0.09 M H_2SO_4 (Reagent Grade, Caledon Laboratory Chemicals) as the electrolyte. The three electrodes included a graphite counter electrode, a reversible hydrogen electrode (RHE) as a reference electrode, and each Si wafer supported catalysts as a working electrode. A flat Cu clip soldered to a Cu wire was used to attach the working electrode to the electrical circuit. A region of ~1 cm × ~2 cm for each substrate was submerged in the electrolyte. The geometric area of each electrode was held constant using an epoxy coating (Devcon® 5 minute® Epoxy) on the remaining sections of the substrate. A pristine, uncoated Pt electrocatalyst, prepared by the same PVD methods, was created to compare the electrochemical activity and durability towards the ORR to the samples coated with a patterned, ultrathin film of Nb_2O_5.

Nitrogen gas (Praxair, 99.998%) was introduced to the cell before electrochemical analysis. To sufficiently evaluate the ability of Nb_2O_5 to protect the Pt surface from degradation, an accelerated stress test (AST) protocol was used to encompass a range of potential degradation mechanisms. All voltages reported are *versus* the reversible hydrogen reference electrode. The sample was initially subjected to cyclic voltammetry (CV) with lower and upper vertices of 0.0 V_{RHE} and 1.25 V_{RHE}, respectively, at a scan rate of 100 mV s^{-1} for 100 cycles to condition the surface. The electrode was subsequently treated with 10 cycles over the same potential range at a scan rate of 50 mV s^{-1} to determine the A_{ecsa} at the beginning of test (BOT) (*i.e.*, after electrochemical conditioning). The A_{ecsa} for each substrate was calculated from an average of the areas associated with hydrogen underpotential deposition or H_{UPD} [obtaining an average from the adsorption region (~0.4 V_{RHE} to 0.05 V_{RHE})] recorded in the final three consecutive CV scans at a rate of 50 mV s^{-1}. In the calculation of the A_{ecsa}, the current arising from the double-layer capacitance was subtracted, and a conversion factor of 210 μC cm^{-2} for Pt was employed to convert the charge calculated from the region of H_{UPD} into the A_{ecsa} values for the Pt catalyst.[58,59] Linear sweep voltammetry (LSV) was performed at 5 mV s^{-1} from 1.1 V_{RHE} to 0.2 V_{RHE} under O_2 saturated conditions before and after the 5000 AST cycles. Electrochemical impedance spectroscopy (EIS) measurements were collected at a DC bias potential of 0.4 V_{RHE} across a frequency range of 100 kHz to 0.1 Hz under N_2 (g) saturated conditions and at 0.9 V_{RHE} under O_2 (g) saturated conditions. The finite transmission-line model developed by the Pickup group was used to analyze EIS data.[60] The AST consisted of cycling the sample from 0.0

V_{RHE} to 1.3 V_{RHE} at a scan rate of 200 mV s^{-1} for a total of 5000 cycles. Post-AST, all samples were characterized in fresh electrolyte and, after 100 scans, performed at a scan rate of 100 mV s^{-1} (0.0 V_{RHE} to 1.25 V_{RHE}). Electrochemical characterization after the AST included slower CV scans, LSV, and EIS using the same parameters as before the AST.

The pristine Pt and Pt coated with patterned Nb_2O_5 layers were probed using potassium ferricyanide. Cyclic voltammetry plots were recorded in 0.1 M KCl (Certified ACS, Fisher Chemical) and 0.01 M $K_3Fe(CN)_6$ (Kodak) from −0.2 $V_{Ag/AgCl}$ to 0.8 $V_{Ag/AgCl}$ at scan rates of 500, 200, 100, 50, and 10 mV s^{-1}.

Author contributions

Collection of scanning electron microscopy images and electrochemical data, electrochemical data analysis, XPS data analysis, contribution to preparation of the manuscript (AMKH), fabrication of patterned electrodes, experimental design, contribution to preparation of the manuscript (JIE), development of procedure for atomic layer deposition, (AP), experimental design and assistance with collection of initial SEM, AFM and KPFM data (MTYP), collection of energy dispersive X-ray spectroscopy data and preparation of sample by focused ion beam lift-out (MWB), collection of AFM and KPFM data, collection of XPS data (AWHL), collection of contact angle measurements, assistance with experimental design, data collection and analysis, and preparation of the manuscript (BDG).

Conflicts of interest

The authors confirm no competing financial interests.

Data availability

The data that support the findings of this study are available from the corresponding author upon reasonable request. Supplementary information: additional analyses of the prepared electrodes by scanning electron microscopy, X-ray photoelectron spectroscopy, water contact angle measurements, electrochemical impedance spectroscopy, and cyclic voltammetry (PDF). See DOI: https://doi.org/10.1039/d5lf00290g.

Acknowledgements

This research was supported in part by the Natural Sciences and Engineering Research Council of Canada (NSERC; Grant No. RGPIN-2020-06522), NSERC CGS-D (Annabelle M. K. Hadley), Mitacs Elevate Grant (J. I. Eastcott; Grant No. IT05187), Mitacs Globalink Program (A. Parakh), and CMC Microsystems (MNT Grant No. 4295). M. W. Bilton thanks Prof. Sarah Haigh and Dr. Matt Smith at the University of Manchester for STEM experimental support using the ThermoFisher Titan 200 kV ChemiSTEM with in column Super-X energy dispersive X-ray spectroscopy (EDS). This work also made use of the 4D LABS at Simon Fraser University (SFU) and the Center for Soft Materials shared facilities supported by the Canada Foundation for Innovation (CFI), British Columbia Knowledge Development Fund (BCKDF), Western Economic Diversification Canada, and SFU.

References

1 K. Yasuda, A. Taniguchi, T. Akita, T. Ioroi and Z. Siroma, Platinum Dissolution and Deposition in the Polymer Electrolyte Membrane of a PEM Fuel Cell as Studied by Potential Cycling, *Phys. Chem. Chem. Phys.*, 2006, **8**(6), 746–752, DOI: 10.1039/B514342J.

2 L. Xing, M. A. Hossain, M. Tian, D. Beauchemin, K. T. Adjemian and G. Jerkiewicz, Platinum Electro-Dissolution in Acidic Media upon Potential Cycling, *Electrocatalysis*, 2014, **5**(1), 96–112, DOI: 10.1007/s12678-013-0167-9.

3 A. A. Topalov, S. Cherevko, A. R. Zeradjanin, J. C. Meier, I. Katsounaros and K. J. J. Mayrhofer, Towards a Comprehensive Understanding of Platinum Dissolution in Acidic Media, *Chem. Sci.*, 2013, **5**(2), 631–638, DOI: 10.1039/C3SC52411F.

4 V. Briega-Martos, K. Stojanovski, M. Zlatar, C. Göllner and S. Cherevko, pH Dependence of Noble Metals Dissolution: Platinum, *Electrochim. Acta*, 2024, **501**, 144793, DOI: 10.1016/j.electacta.2024.144793.

5 F. Forouzandeh, X. Li, D. W. Banham, F. Feng, S. Ye and V. Birss, Understanding the Corrosion Resistance of Meso- and Micro-Porous Carbons for Application in PEM Fuel Cells, *J. Electrochem. Soc.*, 2018, **165**(6), F3230, DOI: 10.1149/2.0261806jes.

6 J. Zhao, Z. Tu and S. H. Chan, Carbon Corrosion Mechanism and Mitigation Strategies in a Proton Exchange Membrane Fuel Cell (PEMFC): A Review, *J. Power Sources*, 2021, **488**, 229434, DOI: 10.1016/j.jpowsour.2020.229434.

7 J. I. Eastcott, A. Parakh, M. T. Y. Paul, A. W. H. Lee, M. W. Bilton and B. D. Gates, Nanoscale Thin Films of Niobium Oxide on Platinum Surfaces: Creating a Platform for Optimizing Material Composition and Electrochemical Stability, *Can. J. Chem.*, 2018, **96**(2), 260–266, DOI: 10.1139/cjc-2017-0595.

8 A. M. Jasim, S. Al-Salihi and Y. Xing, Communication—Platinum and Tin Oxide Dispersed in a Fluffy TiO_2 Nanolayer for Electrocatalytic Reduction of Oxygen, *J. Electrochem. Soc.*, 2020, **167**(11), 116526, DOI: 10.1149/1945-7111/aba96c.

9 D. V. Esposito, Membrane-Coated Electrocatalysts—An Alternative Approach To Achieving Stable and Tunable Electrocatalysis, *ACS Catal.*, 2018, **8**(1), 457–465, DOI: 10.1021/acscatal.7b03374.

10 D. V. Fraga Alvarez, Z. Lin, Z. Shi, A. F. Baxter, E. D. Wang, D. Kuvar, N. Mahmud, M. H. El-Naas, H. D. Abruña, D. A. Muller and D. V. Esposito, Condensed Layer Deposition of Nanoscopic TiO_2 Overlayers on High-Surface-Area Electrocatalysts, *ACS Appl. Mater. Interfaces*, 2024, **16**(19), 25432–25444, DOI: 10.1021/acsami.3c18366.

11 S. Takenaka, H. Matsumori, K. Nakagawa, H. Matsune, E. Tanabe and M. Kishida, Improvement in the Durability of Pt

Electrocatalysts by Coverage with Silica Layers, *J. Phys. Chem. C*, 2007, **111**(42), 15133–15136, DOI: 10.1021/jp076120b.

12 A. M. K. Hadley, S. Gautam and B. D. Gates, Niobium Oxide Coatings on Nanostructured Platinum Electrocatalysts: Benefits and Limitations, *RSC Appl. Interfaces*, 2024, **1**(6), 1334–1347, DOI: 10.1039/D4LF00211C.

13 L. Zhang, L. Wang, C. M. B. Holt, B. Zahiri, Z. Li, K. Malek, T. Navessin, M. H. Eikerling and D. Mitlin, Highly Corrosion Resistant Platinum–Niobium Oxide–Carbon Nanotube Electrodes for the Oxygen Reduction in PEM Fuel Cells, *Energy Environ. Sci.*, 2012, **5**(3), 6156–6172, DOI: 10.1039/C2EE02689A.

14 R. Alipour MoghadamEsfahani, S. K. Vankova, E. B. Easton, I. I. Ebralidze and S. Specchia, A Hybrid Pt/NbO/CNTs Catalyst with High Activity and Durability for Oxygen Reduction Reaction in PEMFC, *Renewable Energy*, 2020, **154**, 913–924, DOI: 10.1016/j.renene.2020.03.029.

15 S.-Y. Huang, P. Ganesan, S. Park and B. N. Popov, Development of a Titanium Dioxide-Supported Platinum Catalyst with Ultrahigh Stability for Polymer Electrolyte Membrane Fuel Cell Applications, *J. Am. Chem. Soc.*, 2009, **131**(39), 13898–13899, DOI: 10.1021/ja904810h.

16 Y. Chen, J. Chen, J. Zhang, Y. Xue, G. Wang and R. Wang, Anchoring Highly Dispersed Pt Electrocatalysts on TiOx with Strong Metal–Support Interactions via an Oxygen Vacancy-Assisted Strategy as Durable Catalysts for the Oxygen Reduction Reaction, *Inorg. Chem.*, 2022, **61**(12), 5148–5156, DOI: 10.1021/acs.inorgchem.2c00329.

17 M. Pourbaix, *Atlas of Electrochemical Equilibria in Aqueous Solutions*, NACE Foundation, Houston, 1974.

18 S. J. Tauster, S. C. Fung, R. T. K. Baker and J. A. Horsley, Strong Interactions in Supported-Metal Catalysts, *Science*, 1981, **211**(4487), 1121–1125.

19 Z. Luo, G. Zhao, H. Pan and W. Sun, Strong Metal–Support Interaction in Heterogeneous Catalysts, *Adv. Energy Mater.*, 2022, **12**(37), 2201395, DOI: 10.1002/aenm.202201395.

20 M. K. Debe, Tutorial on the Fundamental Characteristics and Practical Properties of Nanostructured Thin Film (NSTF) Catalysts, *J. Electrochem. Soc.*, 2013, **160**(6), F522, DOI: 10.1149/2.049306jes.

21 M. K. Debe, A. K. Schmoeckel, G. D. Vernstrom and R. Atanasoski, High Voltage Stability of Nanostructured Thin Film Catalysts for PEM Fuel Cells, *J. Power Sources*, 2006, **161**(2), 1002–1011, DOI: 10.1016/j.jpowsour.2006.05.033.

22 F. D. Speck, F. S. M. Ali, M. T. Y. Paul, R. K. Singh, T. Böhm, A. Hofer, O. Kasian, S. Thiele, J. Bachmann, D. R. Dekel, T. Kallio and S. Cherevko, Improved Hydrogen Oxidation Reaction Activity and Stability of Buried Metal-Oxide Electrocatalyst Interfaces, *Chem. Mater.*, 2020, **32**(18), 7716–7724, DOI: 10.1021/acs.chemmater.0c02048.

23 W.-J. Lee, S. Bera, H. Woo, H. G. Kim, J.-H. Baek, W. Hong, J.-Y. Park, S.-J. Oh and S.-H. Kwon, In Situ Engineering of a Metal Oxide Protective Layer into Pt/Carbon Fuel-Cell Catalysts by Atomic Layer Deposition, *Chem. Mater.*, 2022, **34**(13), 5949–5959, DOI: 10.1021/acs.chemmater.2c00928.

24 S. S. Hardisty, S. Frank, M. Zysler, R. Yemini, A. Muzikansky, M. Noked and D. Zitoun, Selective Catalyst Surface Access through Atomic Layer Deposition, *ACS Appl. Mater. Interfaces*, 2021, **13**(49), 58827–58837, DOI: 10.1021/acsami.1c20181.

25 S. Takenaka, T. Miyazaki, H. Matsune and M. Kishida, Highly Active and Durable Silica-Coated Pt Cathode Catalysts for Polymer Electrolyte Fuel Cells: Control of Micropore Structures in Silica Layers, *Catal. Sci. Technol.*, 2015, **5**(2), 1133–1142, DOI: 10.1039/C4CY01301H.

26 S. Takenaka, N. Susuki, H. Miyamoto, E. Tanabe, H. Matsune and M. Kishida, Highly Durable Carbon Nanotube-Supported Pd Catalysts Covered with Silica Layers for the Oxygen Reduction Reaction, *J. Catal.*, 2011, **279**(2), 381–388, DOI: 10.1016/j.jcat.2011.02.008.

27 S. Takenaka, H. Miyamoto, Y. Utsunomiya, H. Matsune and M. Kishida, Catalytic Activity of Highly Durable Pt/CNT Catalysts Covered with Hydrophobic Silica Layers for the Oxygen Reduction Reaction in PEFCs, *J. Phys. Chem. C*, 2014, **118**(2), 774–783, DOI: 10.1021/jp407928m.

28 J. E. Robinson, N. Y. Labrador, H. Chen, B. E. Sartor and D. V. Esposito, Silicon Oxide-Encapsulated Platinum Thin Films as Highly Active Electrocatalysts for Carbon Monoxide and Methanol Oxidation, *ACS Catal.*, 2018, **8**(12), 11423–11434, DOI: 10.1021/acscatal.8b03626.

29 K. Lu, X. Kong, J. Cai, S. Yu and X. Zhang, Review on Supported Metal Catalysts with Partial/Porous Overlayers for Stabilization, *Nanoscale*, 2023, **15**(18), 8084–8109, DOI: 10.1039/D3NR00287J.

30 X. M. C. Ta, T. Trân-Phú, J. A. Yuwono, T. K. A. Nguyen, A. D. Bui, T. N. Truong, L. Chang, E. Magnano, R. Daiyan, A. N. Simonov and A. Tricoli, Optimal Coatings of Co_3O_4 Anodes for Acidic Water Electrooxidation, *Small*, 2024, **20**(39), 2304650, DOI: 10.1002/smll.202304650.

31 M. Kwak, K. Ojha, M. Shen and S. W. Boettcher, Electrically Insulated Catalyst–Ionomer Anode Interfaces toward Durable Alkaline Membrane Electrolyzers, *ACS Energy Lett.*, 2024, **9**(3), 1025–1034, DOI: 10.1021/acsenergylett.3c02620.

32 Y. Xue, Z. S. Fishman, Y. Wang, Z. Pan, X. Shen, R. Yanagi, G. S. Hutchings, M. Liu, S. Zheng, Y. Zhang, E. I. Altman and S. Hu, Hydrogen Evolution Activity Tuning via Two-Dimensional Electron Accumulation at Buried Interfaces, *J. Mater. Chem. A*, 2019, **7**(36), 20696–20705, DOI: 10.1039/C9TA07123G.

33 S. Chung, M. Choun, B. Jeong, J. K. Lee and J. Lee, Atomic Layer Deposition of Ultrathin Layered TiO_2 on Pt/C Cathode Catalyst for Extended Durability in Polymer Electrolyte Fuel Cells, *J. Energy Chem.*, 2016, **25**(2), 258–264, DOI: 10.1016/j.jechem.2016.01.010.

34 Y. Li, Z. Ding, Y. Zhou, Z. Liu, L. Huang, L. Chen and X. Feng, High O_2 Tolerant Metal-Based Catalysts for Selective H_2O_2 Reduction by Constructing an Ultra-Thin Oxide Passivation Layer, *Mater. Horiz.*, 2025, **12**, 6938–6944, DOI: 10.1039/D5MH00716J.

35 P. Poodt, D. C. Cameron, E. Dickey, S. M. George, V. Kuznetsov, G. N. Parsons, F. Roozeboom, G. Sundaram and A. Vermeer, Spatial Atomic Layer Deposition: A Route towards Further Industrialization of Atomic Layer Deposition, *J. Vac. Sci. Technol., A*, 2011, **30**(1), 010802, DOI: 10.1116/1.3670745.

36 H. Zhang, C. Canlas, A. Jeremy Kropf, J. W. Elam, J. A. Dumesic and C. L. Marshall, Enhancing the Stability of Copper Chromite Catalysts for the Selective Hydrogenation of Furfural with ALD Overcoating (II) – Comparison between TiO_2 and Al_2O_3 Overcoatings, *J. Catal.*, 2015, **326**, 172–181, DOI: 10.1016/j.jcat.2015.03.017.

37 T. M. Onn, S. Zhang, L. Arroyo-Ramirez, Y.-C. Chung, G. W. Graham, X. Pan and R. J. Gorte, Improved Thermal Stability and Methane-Oxidation Activity of Pd/Al_2O_3 Catalysts by Atomic Layer Deposition of ZrO_2, *ACS Catal.*, 2015, **5**(10), 5696–5701, DOI: 10.1021/acscatal.5b01348.

38 T. M. Onn, L. Arroyo-Ramirez, M. Monai, T.-S. Oh, M. Talati, P. Fornasiero, R. J. Gorte and M. M. Khader, Modification of Pd/CeO_2 Catalyst by Atomic Layer Deposition of ZrO_2, *Appl. Catal., B*, 2016, **197**, 280–285, DOI: 10.1016/j.apcatb.2015.12.028.

39 J. Lu, B. Fu, M. C. Kung, G. Xiao, J. W. Elam, H. H. Kung and P. C. Stair, Coking- and Sintering-Resistant Palladium Catalysts Achieved Through Atomic Layer Deposition, *Science*, 2012, **335**(6073), 1205–1208, DOI: 10.1126/science.1212906.

40 T. Fujimura, W. Hikima, Y. Fukunaka and T. Homma, Analysis of the Effect of Surface Wettability on Hydrogen Evolution Reaction in Water Electrolysis Using Micro-Patterned Electrodes, *Electrochem. Commun.*, 2019, **101**, 43–46, DOI: 10.1016/j.elecom.2019.02.018.

41 H. Cho, S. Moon Kim, Y. Sik Kang, J. Kim, S. Jang, M. Kim, H. Park, J. Won Bang, S. Seo, K.-Y. Suh, Y.-E. Sung and M. Choi, Multiplex Lithography for Multilevel Multiscale Architectures and Its Application to Polymer Electrolyte Membrane Fuel Cell, *Nat. Commun.*, 2015, **6**(1), 8484, DOI: 10.1038/ncomms9484.

42 *CRC Handbook of Chemistry and Physics*, ed. W. M. Haynes, CRC Press, Boca Raton, 95th edn, 2014, DOI: 10.1201/b17118.

43 A. Dacca, G. Gemme, L. Mattera and R. Parodi, XPS Characterization of Niobium for RF Cavities, *Part. Accel.*, 1998, **60**, 103–120.

44 S. J. A. Zaidi, J. C. Park, J. W. Han, J. H. Choi, M. A. Ali, M. A. Basit and T. J. Park, Interfaces in Atomic Layer Deposited Films: Opportunities and Challenges, *Small Sci.*, 2023, **3**(10), 2300060, DOI: 10.1002/smsc.202300060.

45 D. M. Mattox, Preparation and Cleaning of Vacuum Surfaces, In *Handbook of Vacuum Science and Technology*, ed. D. M. Hoffman, B. Singh, J. H. Thomas and J. H. Thomas, Academic Press, San Diego, 1998, ch. 4.9, pp. 553–606, DOI: 10.1016/B978-012352065-4/50070-5.

46 A. Berman, Water Vapor in Vacuum Systems, *Vacuum*, 1996, **47**(4), 327–332, DOI: 10.1016/0042-207X(95)00246-4.

47 J. B. Peri, Infrared and Gravimetric Study of the Surface Hydration of γ-Alumina, *J. Phys. Chem.*, 1965, **69**(1), 211–219, DOI: 10.1021/j100885a032.

48 K. J. J. Mayrhofer, D. Strmcnik, B. B. Blizanac, V. Stamenkovic, M. Arenz and N. M. Markovic, Measurement of Oxygen Reduction Activities via the Rotating Disc Electrode Method: From Pt Model Surfaces to Carbon-Supported High Surface Area Catalysts, *Electrochim. Acta*, 2008, **53**(7), 3181–3188, DOI: 10.1016/j.electacta.2007.11.057.

49 C. S. Abraham, M. Anand, S. R. Kelly, Z. Wang and J. K. Nørskov, Analysing Oxygen Reduction Electrocatalysis on Transition Metal Doped Niobium Oxide(110), *Phys. Chem. Chem. Phys.*, 2022, **24**(28), 17116–17120, DOI: 10.1039/D1CP05725A.

50 T. J. Davies, C. E. Banks and R. G. Compton, Voltammetry at Spatially Heterogeneous Electrodes, *J. Solid State Electrochem.*, 2005, **9**(12), 797–808, DOI: 10.1007/s10008-005-0699-x.

51 B. A. Brookes, T. J. Davies, A. C. Fisher, R. G. Evans, S. J. Wilkins, K. Yunus, J. D. Wadhawan and R. G. Compton, Computational and Experimental Study of the Cyclic Voltammetry Response of Partially Blocked Electrodes. Part 1. Nonoverlapping, Uniformly Distributed Blocking Systems, *J. Phys. Chem. B*, 2003, **107**(7), 1616–1627, DOI: 10.1021/jp021810v.

52 N. Arulmozhi, D. Esau, R. P. Lamsal, D. Beauchemin and G. Jerkiewicz, Structural Transformation of Monocrystalline Platinum Electrodes upon Electro-Oxidation and Electro-Dissolution, *ACS Catal.*, 2018, **8**(7), 6426–6439, DOI: 10.1021/acscatal.8b00319.

53 M. Ruge, J. Drnec, B. Rahn, F. Reikowski, D. A. Harrington, F. Carlà, R. Felici, J. Stettner and O. M. Magnussen, Structural Reorganization of Pt(111) Electrodes by Electrochemical Oxidation and Reduction, *J. Am. Chem. Soc.*, 2017, **139**(12), 4532–4539, DOI: 10.1021/jacs.7b01039.

54 L. Kim, C. G. Chung, Y. W. Sung and J. S. Chung, Dissolution and Migration of Platinum after Long-Term Operation of a Polymer Electrolyte Fuel Cell under Various Conditions, *J. Power Sources*, 2008, **183**(2), 524–532, DOI: 10.1016/j.jpowsour.2008.05.062.

55 K. Sasaki, L. Zhang and R. R. Adzic, Niobium Oxide-Supported Platinum Ultra-Low Amount Electrocatalysts for Oxygen Reduction, *Phys. Chem. Chem. Phys.*, 2007, **10**(1), 159–167, DOI: 10.1039/B709893F.

56 L. Zhang, L. Wang, C. M. B. Holt, T. Navessin, K. Malek, M. H. Eikerling and D. Mitlin, Oxygen Reduction Reaction Activity and Electrochemical Stability of Thin-Film Bilayer Systems of Platinum on Niobium Oxide, *J. Phys. Chem. C*, 2010, **114**(39), 16463–16474, DOI: 10.1021/jp104306j.

57 C.-H. Chen, A. Halford, M. Walker, C. Brennan, S. C. S. Lai, D. J. Fermin, P. R. Unwin and P. Rodriguez, Electrochemical Characterization and Regeneration of Sulfur Poisoned Pt Catalysts in Aqueous Media, *J. Electroanal. Chem.*, 2018, **816**, 138–148, DOI: 10.1016/j.jelechem.2018.03.015.

58 T. J. Schmidt, H. A. Gasteiger, G. D. Stäb, P. M. Urban, D. M. Kolb and R. J. Behm, Characterization of High-Surface-Area

Electrocatalysts Using a Rotating Disk Electrode Configuration, *J. Electrochem. Soc.*, 1998, **145**(7), 2354, DOI: 10.1149/1.1838642.

59 T. Biegler, D. A. J. Rand and R. Woods, Limiting Oxygen Coverage on Platinized Platinum; Relevance to Determination of Real Platinum Area by Hydrogen Adsorption, *J. Electroanal. Chem. Interfacial Electrochem.*, 1971, **29**(2), 269–277, DOI: 10.1016/S0022-0728(71)80089-X.

60 E. B. Easton and P. G. Pickup, An Electrochemical Impedance Spectroscopy Study of Fuel Cell Electrodes, *Electrochim. Acta*, 2005, **50**(12), 2469–2474, DOI: 10.1016/j.electacta.2004.10.074.